STATE OF THE CLIMATE IN 2017

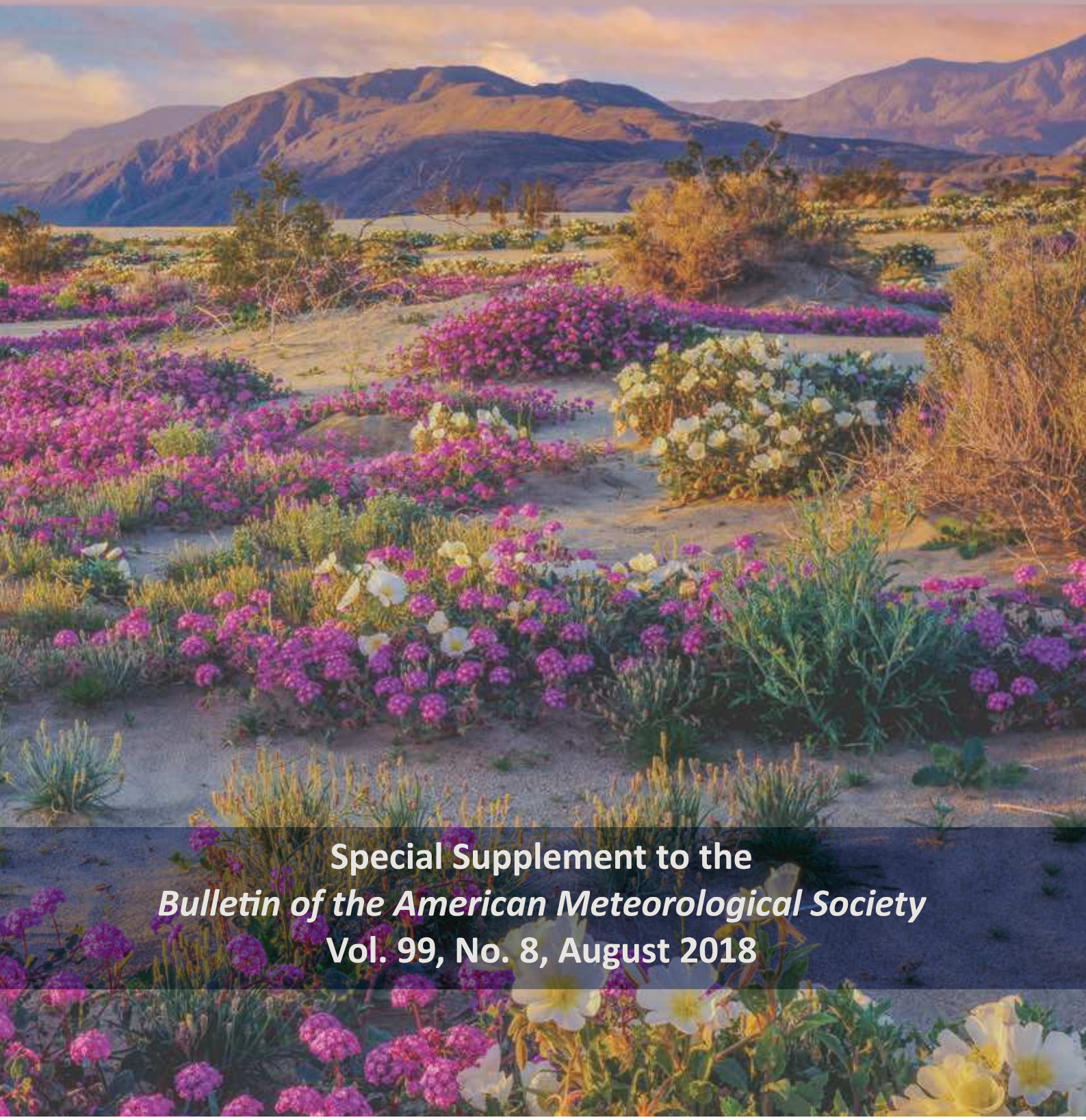

Special Supplement to the
Bulletin of the American Meteorological Society
Vol. 99, No. 8, August 2018

STATE OF THE CLIMATE IN 2017

Editors

Jessica Blunden
Derek S. Arndt
Gail Hartfield

Chapter Editors

Peter Bissolli
Howard J. Diamond
Robert J. H. Dunn
Catherine Ganter
Nadine Gobron
Martin O. Jeffries
Gregory C. Johnson
Tim Li
Ademe Mekonnen
Emily Osborne
Jacqueline A. Richter-Menge
Ahira Sánchez-Lugo
Ted A. Scambos
Carl J. Schreck III
Sharon Stammerjohn
Diane M. Stanitski
Kate M. Willett

Technical Editor

Mara Sprain

***BAMS* Special Editor for Climate**

Richard Rosen

American Meteorological Society

Cover credits:

Front: ©Ron_ Thomas/Spring desert wildflowers in Anza Borrego Desert State Park, CA/Getty Images.

Back: Smoke and Fire in Southern California: Thick smoke was streaming from several fires in Southern California when the Moderate Resolution Imaging Spectroradiometer (MODIS) on NASA's *Terra* satellite acquired a natural-color image in the afternoon on December 5, 2017. On the same day, the Multi Spectral Imager (MSI) on the European Space Agency's Sentinel-2 satellite captured the data for a false-color image of the burn scar. Active fires appear orange; the burn scar is brown. Unburned vegetation is green; developed areas are gray. The Sentinel-2 image is based on observations of visible, shortwave infrared, and near infrared light.

NASA Earth Observatory images by Joshua Stevens, using MODIS data from LANCE/EOSDIS Rapid Response and modified Copernicus Sentinel data (2017) processed by the European Space Agency. Story by Adam Voiland.
Instrument(s):
Terra - MODIS
Sentinel-2

How to cite this document:

Citing the complete report:

Blunden, J., D. S. Arndt, and G. Hartfield , Eds., 2018: State of the Climate in 2017. *Bull. Amer. Meteor. Soc.*, **99** (8), S*i*–S310, doi:10.1175/2018BAMSStateoftheClimate.1.

Citing a chapter (example):

Richter-Menge, J., M. O. Jeffries, and E. Osborne, Eds., 2018: The Arctic [in "State of the Climate in 2017"]. *Bull. Amer. Meteor. Soc.*, **99** (8), S143–173, doi:10.1175/2018BAMSStateoftheClimate.1.

Citing a section (example):

Osborne, E., T. Cronin, and J. Farmer, 2018: Paleoclimate records: Providing context and understanding of current Arctic change [in "State of the Climate in 2017"]. *Bull. Amer. Meteor. Soc.*, **99** (8), S150–S152, doi:10.1175/2018BAMSStateoftheClimate.1.

Chl*a* distributions and responses to climatic events. The time series also demonstrates the high level of consistency between the overlapping periods of the SeaWiFS and MODISA missions, lending confidence to interpretation of the multimission record.

Chl*a* monthly anomalies within the PSO (Fig. 3.26b) show variations of ±15% (±0.02 mg m^{-3}) over the multimission time series. For 2017, these anomalies were relatively constant and slightly elevated (+0.005 mg m^{-3}, on average) relative to the long-term mean, consistent with the weak La Niña conditions as discussed previously. The link between ENSO variability and mean Chl*a* response in the PSO is demonstrated by the correspondence of anomaly trends with the multivariate ENSO index (MEI; Wolter and Timlin 1998; Fig. 3.26b, green diamonds, presented in the inverse to illustrate the covariation). From 1997 through 2017, monthly anomalies in Chl*a* concentration within the PSO continue to track large-scale climate oscillations as captured by the MEI (Fig. 3.26b), with some notable deviations in the 2002–06 period.

Variability and trends in Chl*a* reflect both adjustments in phytoplankton biomass and physiology (or health). Both of these properties are mechanistically linked to physical properties of the upper ocean, as well as ecological relationships between phytoplankton and their zooplankton predators. Unraveling the diversity and covariation of factors that influence Chl*a* concentrations is essential for correctly interpreting the implications of Chl*a* anomalies on ocean biogeochemistry and food webs. For example, inverse relationships between Chl*a* and SST can emerge from changes in either mixed-layer light levels or vertical nutrient flux, but these two mechanisms have opposite implications on phytoplankton NPP (Behrenfeld et al. 2016). An additional complication is that measured changes in ocean color often contain a contribution from colored dissolved organic matter (Siegel et al. 2005) that can be mistakenly attributed to changes in Chl*a* (Siegel et al. 2013). Thus, while the satellite record of ocean color continues to provide critical insights on global processes, ongoing effort and new approaches are needed to fully understand the story these data are telling regarding relationships between climate and marine ecosystems.

j. Global ocean carbon cycle—R. A. Feely, R. Wanninkhof, B. R. Carter, P. Landschützer, A. Sutton, and J. A. Triñanes

As a consequence of humankind's collective release of CO_2 emissions into the atmosphere from fossil fuel burning, cement production, and land use changes over the last 250 years, referred to as Anthropogenic CO_2 (C_{anth}), the atmospheric CO_2 has risen from preindustrial levels of about 278 ppm (parts per million) to about 405 ppm (see Section 2g1). The atmospheric concentration of CO_2 is now higher than has been observed on Earth for at least the last 800 000 years (Lüthi et al. 2008). As discussed in previous *State of the Climate* reports, the global ocean is a major sink for C_{anth}. Here the discussion is updated to include recent estimates of that sink. Over the last decade the global ocean has continued to take up a substantial fraction of the anthropogenic carbon (C_{anth}) emissions and therefore is a major mediator of global climate change. Of the 10.7 (±0.9) Pg C yr^{-1} C_{anth} released during the period 2007–16, about 2.4 (±0.5) Pg C yr^{-1} (26%) accumulated in the ocean, 3.0 (±0.8) Pg C yr^{-1} (30%) accumulated on land, and 4.7 (±0.1) Pg C yr^{-1} (43%) remained in the atmosphere with an imbalance of 0.6 Pg C yr^{-1} (Le Quéré et al. 2018). This decadal ocean carbon uptake estimate is a consensus view based on a combination of measured decadal inventory changes, models, and global air–sea CO_2 flux estimates based on surface ocean partial pressure of CO_2 (pCO_2) measurements. Using ocean general circulation models that include biogeochemical parameterizations (OBGCMs) and inverse models that are validated with observations-based air–sea exchange fluxes and basin-scale ocean inventories, Le Quéré et al. (2018) have demonstrated that the oceanic anthropogenic carbon sink has grown from 1.0 (±0.5) Pg C yr^{-1} in the decade of the 1960s to 2.6 (±0.5) Pg C yr^{-1} in 2016. Air–sea CO_2 flux studies reported here indicate an ocean uptake of C_{anth} of 2.6 Pg C yr^{-1} for 2017.

1) Air–sea carbon dioxide fluxes

Ocean uptake of C_{anth} can be estimated from the net air–sea CO_2 flux derived from the bulk flux formula with air–sea differences in CO_2 partial pressure (ΔpCO_2) and gas transfer coefficients as input. A steady contribution of carbon from riverine runoff, originating from organic and inorganic detritus from land, estimated at 0.45 Pg C yr^{-1} (Jacobson et al. 2007) is included to obtain the C_{anth} uptake by the ocean. The data sources for pCO_2 are annual updates of surface water pCO_2 observations from the Surface Ocean CO_2 Atlas (SOCAT) composed of mooring and ship-based observations (Bakker et al. 2016) and the LDEO database with ship-based observations (Takahashi et al. 2018). The increased observations and improved mapping techniques such as neural network methods and self-organizing maps (Landschützer et al. 2013, 2014; Rödenbeck et al. 2015) provide global pCO_2 fields on a 1° latitude × 1° longitude grid at monthly time scales annually. This allows investigation of

variability on subannual to decadal time scales. The ΔpCO_2 and a parameterization of the gas transfer with wind described in Wanninkhof (2014) are used to calculate the air–sea CO_2 fluxes.

The monthly 2017 ΔpCO_2 maps are based on an observation-based neural network approach of Landschützer et al. (2013, 2014). The 2017 values are projections based on surface temperature, sea surface salinity, climatological mixed-layer depth, satellite chlorophyll-α, atmospheric CO_2, and the neural network for pCO_{2w} developed from the data from the previous decade. Moreover, winds from 2016 are used. A comparison of the 2016 air–sea estimate using wind speeds from 2015, as presented in last year's *State of the Climate* report, and the 2016 global flux using measured 2016 pCO_{2w} and 2016 winds show agreement on a global scale to within 0.1 Pg C yr^{-1}. Changes in winds over time have a small effect on global air–sea CO_2 fluxes (Wanninkhof and Triñanes 2017). The C_{anth} fluxes from 1982 to 2017 suggests a decreasing ocean sink in the first part of the record and a strong increase from 2001 onward that continued into 2017 (Fig. 3.27). The amplitude of seasonal variability is large (≈ 1 Pg C) compared to the long-term trend with minimum uptake in the June–September timeframe. The C_{anth} air–sea flux of 2.6 Pg C yr^{-1} in 2017 is 36% above the 2005–15 average of 1.9 (±0.5) Pg C yr^{-1}.

The average fluxes in 2017 (Fig. 3.28a) show the characteristic pattern of effluxes in the tropical regions and uptake at higher latitudes. The region with largest efflux is the equatorial Pacific. Localized hotspots of upwelling include the Arabian Sea, off the coast of Mauritania, and the Peruvian upwelling system. Large sinks are observed poleward of the subtropical fronts, and the frontal position determines the location of the maximum that is farther south in the Pacific sector of the Southern Ocean compared to the other basins.

In the Northern Hemisphere, there is a significant asymmetry in the sub-Arctic gyre with the North Atlantic being a large sink while the North Pacific is a source of CO_2. Ocean carbon uptake anomalies (Fig. 3.28b) in 2017 relative to a 1995–2015 average are attributed to the increasing ocean CO_2 uptake with time (Fig. 3.27) and to variations in large-scale climate modes. The air–sea flux trend since 2000 is −0.8 Pg C $decade^{-1}$, which leads to predominantly negative flux anomalies (greater ocean uptake). Despite this strong trend there are several regions

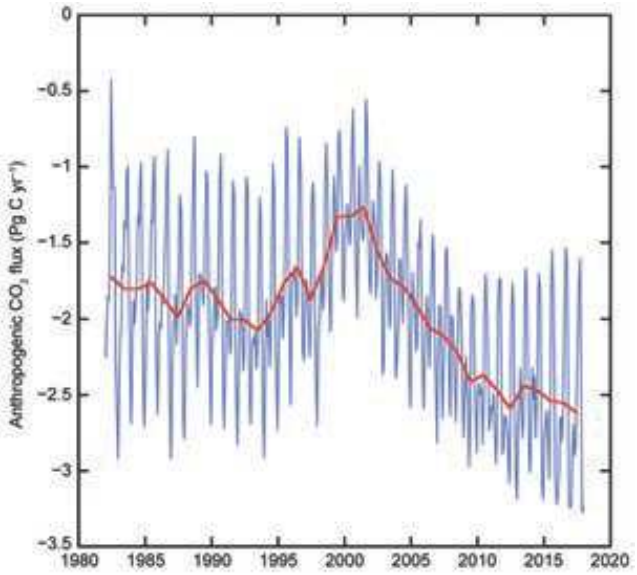

Fig. 3.27. Global annual (red line) and monthly (blue line) C_{anth} fluxes (Pg C yr^{-1}) for 1982 to 2017. Negative values indicate CO_2 uptake by the ocean.

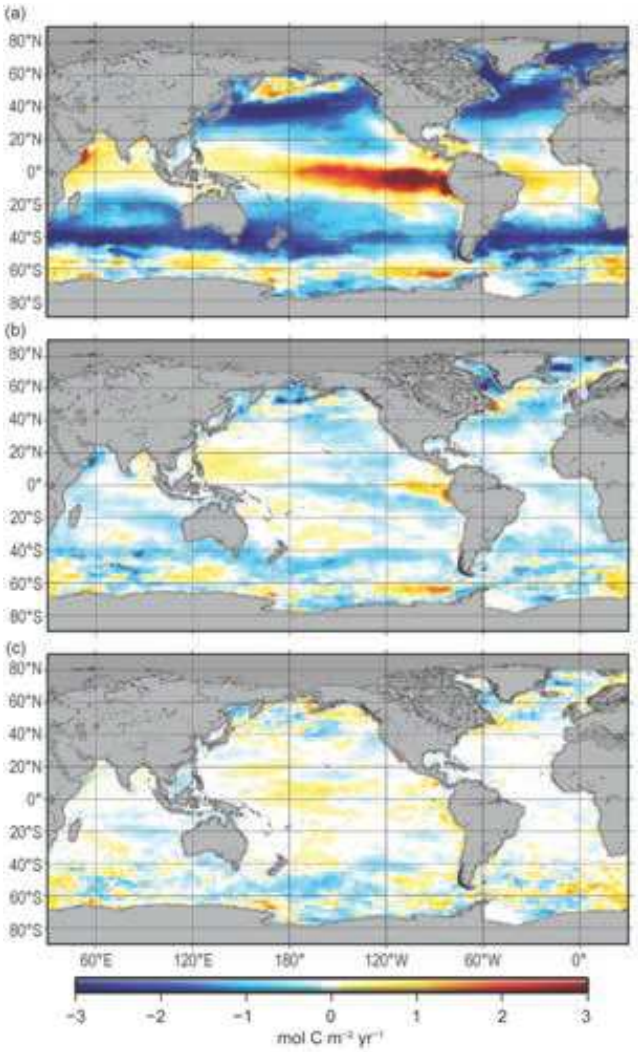

Fig. 3.28. Global map of (a) net air–sea CO_2 fluxes for 2017, (b) net air–sea CO_2 flux anomalies for 2017 relative to a 1995–2015 average, and (c) net air–sea CO_2 flux anomalies for 2017 minus 2016 values following the method of Landschützer et al. (2013), all in mol C m^{-2} yr^{-1}.

showing positive anomalies for 2017, notably the eastern equatorial and western tropical Pacific. The increased effluxes in the eastern equatorial Pacific are related to a predominant positive sign of the ENSO index and the associated switch from the 2015/16 El Niño to the weak La Niñas at the ends of 2016 and 2017. Weaker effluxes in the western tropical Pacific are related to strongly positive PDO values over the past three years that have persisted into the first half of 2017 and associated warmer SSTs.

The differences between the air–sea CO_2 fluxes in 2017 compared to 2016 (Fig. 3.28c) are relatively small. The increase in CO_2 effluxes in the western tropical Pacific from 2016 to 2017 is associated with anomalously warm temperatures in this region in 2017. The Southern Ocean (south of 40°S) shows a bimodal pattern with increasing fluxes in the Pacific and decreasing fluxes in the Atlantic for 2017 compared to 2016. This broadly corresponds to the temperature anomalies in this region, with greater uptake in 2017 associated with warmer temperatures attributed to less upwelling of cold high-CO_2 waters in the western and central Pacific sector of the Southern Ocean and overall colder patterns in the eastern Pacific, Indian, and Atlantic sectors of the Southern Ocean associated with increased ventilation and associated effluxes. The alternating patterns of stronger and weaker uptake in the Southern Ocean are in accord with an asymmetric distribution of the atmospheric pressure systems moving around the Southern Ocean associated with the Antarctic Circumpolar Wave (Landschützer et al. 2015).

Many of the pCO_2 and flux anomalies can be attributed to variations in large-scale climate modes and associated physical anomalies, notably temperature, but the causality is often complex. For example, the behavior of pCO_2 with respect to temperature includes competing processes: thermodynamics dictate decreasing pCO_2 with decreasing SST, but waters originating from the deep with a cold temperature signal will have a high pCO_2. Moreover, the drawdown of pCO_2 due to biology is often associated with increasing temperature, but this depends on region and season.

The strong trend of increasing CO_2 uptake since 2002 has continued through 2017 with an increase of 0.1 Pg C above the 2016 estimate. This increase is well within the uncertainty of the estimate, but it is within the overall expectation that the ocean will remain an increasing sink as long as atmospheric CO_2 levels continue to rise. The sequestration of CO_2 by the ocean partially mitigates the atmospheric CO_2 rise but it comes at a cost of increased acidification of surface and subsurface waters.

2) Ocean acidification

To date, the global oceans have absorbed approximately 150 (±20) Gt C of the total anthropogenic carbon dioxide emissions (Le Quéré et al. 2018). This uptake has caused an increase of ocean acidity in a process referred to as anthropogenic ocean acidification (OA). Models indicate that over the last two-and-a-half centuries, the pH in open-ocean surface waters has decreased by about 0.11 units, equivalent to about a 29% increase in the hydrogen ion (H+) concentration (Gattuso et al. 2015). This absorption of anthropogenic carbon is beneficial in slowing the rise of atmospheric carbon dioxide. However, the ocean's uptake of carbon dioxide is having negative impacts on ocean chemistry and biology. Time series measurements, hydrographic surveys, and modeling studies have revealed that the changes in seawater chemistry resulting from the absorption of CO_2 are lowering seawater pH. For example, the time series data at Ocean Station ALOHA shows an average pH decrease of approximately 0.02 units decade^{-1} in the northeast Pacific (Fig. 3.29).

The long-term trend at Ocean Station ALOHA shows an increasing rate of increase of pCO_2 of 2.0 (±0.1) µatm yr^{-1} (Fig. 3.29a) while pH of ocean surface waters has already decreased by about 0.0016 yr^{-1}, with no apparent long-term change in annual CO_2 influx (Fig. 3.29b; Sutton et al. 2017). The increase in surface ocean CO_2 over recent decades is consistent with the atmospheric increase within the statistical limits of the measurements.

3) Carbon inventories

The Global Ocean Ship-based Hydrographic Investigations Program (GO-SHIP) is providing new information about the uptake and storage of carbon within the ocean interior by determining the change in measured dissolved inorganic carbon (DIC) and C_{anth} concentrations between decadal cruise reoccupations. During the 2017/18 timeframe, a new set of measurements, including DIC, were finalized along the P18 line extending from San Diego south to Antarctica and collected along the P06 line extending from Australia east to Chile. A synthesis of estimates of C_{anth} storage along these sections and other recently measured Pacific sections is currently underway. While results are preliminary, the dominant signal is a clear and continuous increase in C_{anth} storage, especially in the least-dense and most well-ventilated shallower parts of the ocean (Fig. 3.30a). This C_{anth} storage is increasing ocean acidity, decreasing ocean

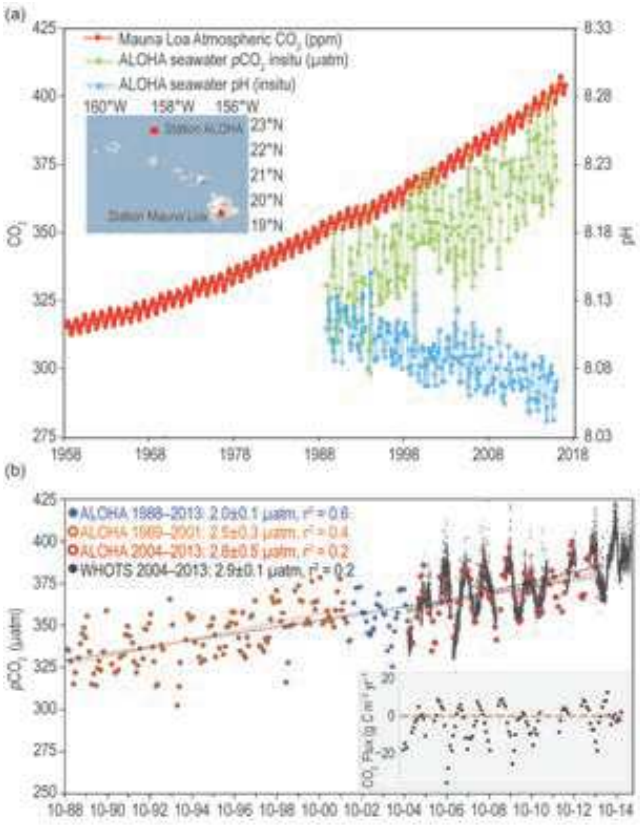

Fig. 3.29. (a) Time series of atmospheric CO_2 at Mauna Loa (ppm), surface ocean pCO_2 (µatm) and pH at Ocean Station ALOHA in the subtropical North Pacific Ocean. Mauna Loa data: (ftp://aftp.cmdl.noaa.gov/products/trends/co2/co2_mm_mlo.txt); HOTS/ALOHA data: University of Hawaii (http://hahana.soest.hawaii.edu/hot/products/HOT_surface_CO2.txt). (b) Surface ocean pCO_2 (µatm) and rates of change from Station ALOHA 1988–2013 (blue), 1989–2001 (orange), 2004–13 (red), and the adjacent WHOTS buoy 2004–13 (black) and (shaded inset) CO_2 flux (g C m^{-2} yr^{-1}) from WHOTS buoy observations 2004–15 (after Sutton et al. 2017).

pH (Fig. 3.30b), and decreasing carbonate mineral saturation states. For this comparison, anthropogenic CO_2 storage rates—estimated from decadal measurements using methods described by Carter et al. (2017)—are used directly and, in some regions, extrapolated in time to estimate patterns of C_{anth} storage since 1994. These storages are added to the 1994 global C_{anth} climatology of Sabine et al. (2004) as gridded by Key et al. (2004).

As also found in recent studies in the Atlantic (Woosley et al. 2016) and Pacific (Carter et al. 2017), these preliminary results suggest that Pacific storage rates have been increasing since ~2005 despite the tendency of water with more CO_2 to absorb smaller fractions of atmospheric C_{anth} increases (due to the decreasing buffering capacity of seawater). The observed storage increases are attributable to continued rapid atmospheric CO_2 growth and changes in mixing and ventilation within the ocean interior. The largest storages per unit area are found in high-latitude deep water formation regions such as the North Atlantic (Woosley et al. 2016), though the majority of the C_{anth} inventory is stored in the subtropics due to the vast size of that region. Upwelling regions near the equator, in the North Pacific, and in the Southern Ocean south of the Antarctic Circumpolar Current have lower decadal storages per unit area (e.g., the dark colors on the lower right Section in Fig. 3.30a). In these regions, upwelling of deep waters that have been isolated from the atmosphere for all or some of the industrial era displace the better-ventilated, higher C_{anth} intermediate depth waters. A preliminary estimate of the decadal changes suggests that the Pacific basin stored 8.2 Pg C between 1995 and 2005 and 9.8 Pg C between 2005 and 2015.

Ocean acidification, or the impact of C_{anth} on pH, has a similar global pattern to the net C_{anth} storage, though the pH decrease is amplified in seawater with

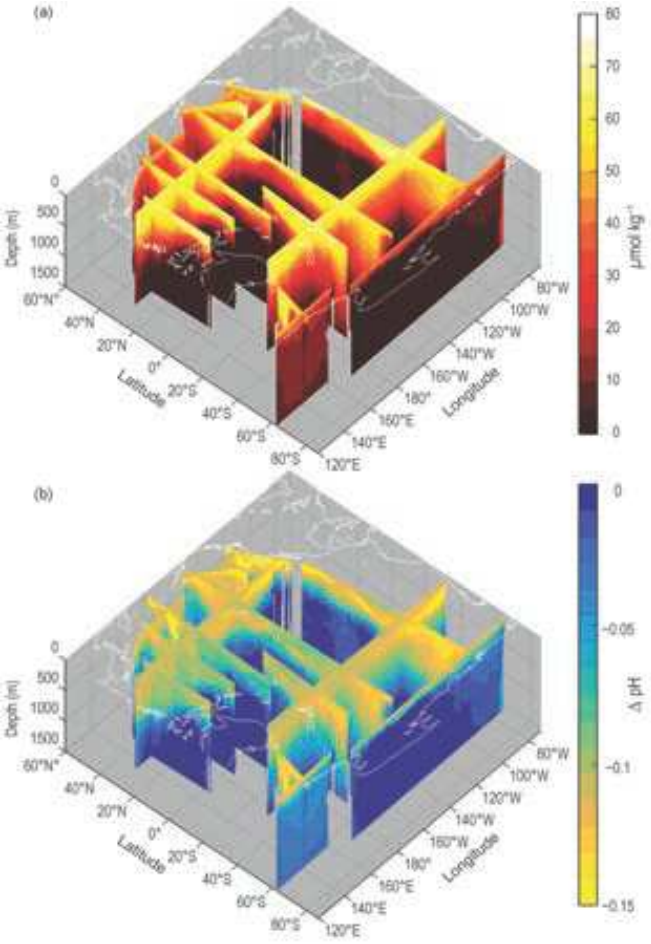

Fig. 3.30. Preliminary estimates of (a) anthropogenic carbon (C_{anth}; µmol kg^{-1}) along hydrographic sections in the Pacific interpolated (or extrapolated) in time to the year 2015 and (b) the net impact of this C_{anth} on pH.

naturally high accumulated DIC from respiration by marine organisms. Such waters have a reduced buffer capacity due to their naturally high carbon concentrations, so the ongoing C_{anth} storage has an enhanced impact on acidification. This effect can be seen in the nearly global subsurface ΔpH magnitude maximum, which is especially notable off the US West Coast where unusually high-DIC waters upwell near the surface (Fig. 3.30b).